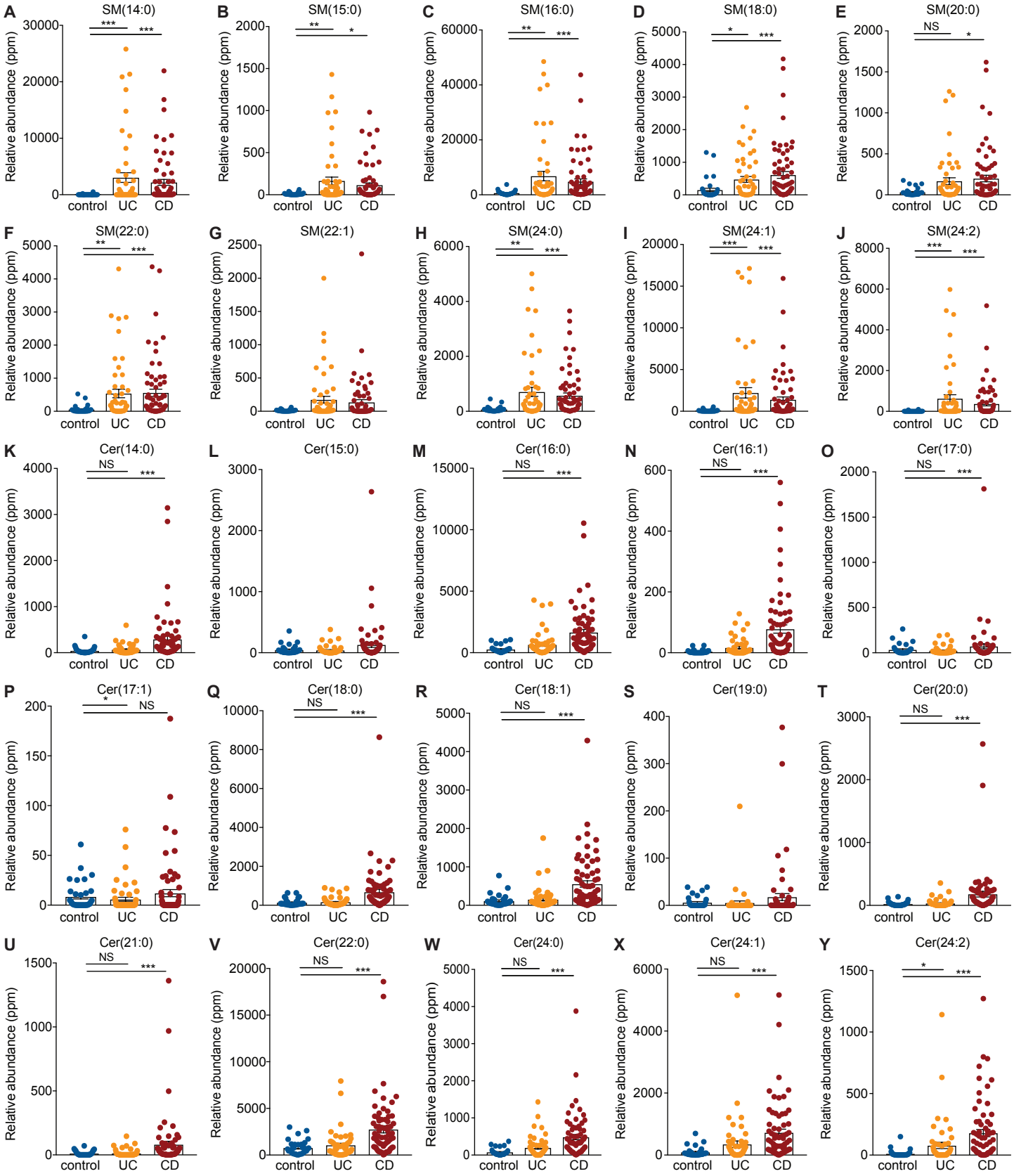

Figure S1: Host-produced ceramide and sphingomyelin abundances are significantly altered in stool of patients with IBD. Related to Figure 1. A total of 25 host-produced ceramide and sphingomyelin metabolites were annotated and quantified in stool samples from non-IBD controls (blue) and subjects with Crohn's disease (CD; red) or ulcerative colitis (UC; yellow). For each stool sample for which the data existed, box-plots were created describing the abundances (ppm) of **(A)** sphingomyelin (14:0), **(B)** sphingomyelin (15:0), **(C)** sphingomyelin (16:0), **(D)** sphingomyelin (18:0), **(E)** sphingomyelin (20:0), **(F)** sphingomyelin (22:0), **(G)** sphingomyelin (22:1), **(H)** sphingomyelin (24:0), **(I)** sphingomyelin (24:1), **(J)** sphingomyelin (24:2), **(K)** ceramide (14:0), **(L)** ceramide (15:0), **(M)** ceramide (16:0), **(N)** ceramide (16:1), **(O)** ceramide (17:0), **(P)** ceramide (17:1) **(Q)** ceramide (18:0), **(R)** ceramide (18:1), **(S)** ceramide (19:0), **(T)** ceramide (20:0), **(U)** ceramide (21:0), **(V)** ceramide (22:0), **(W)** ceramide (24:0), **(X)** ceramide (24:1), and **(Y)** ceramide (24:2). Bars represent the mean abundance of each sample. Statistical significance was determined by analysis of the FDR (*FDR<0.05; **FDR<0.01; ***FDR<0.001). NS, not significant. Error bars are +/- SEM.

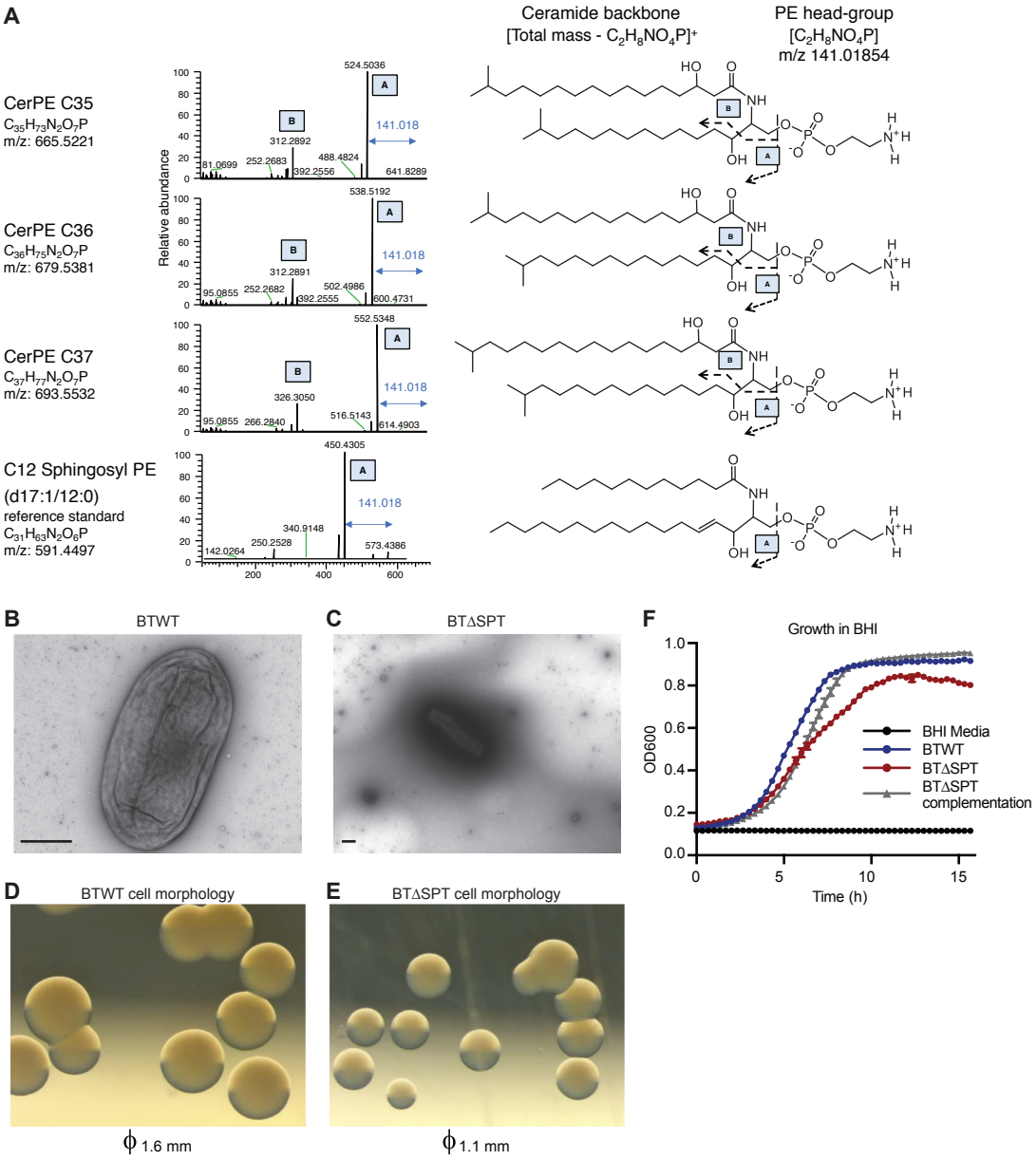

Figure S2: Genetic deletion of the putative serine palmitoyltransferase enzyme in *B. thetaiotaomicron* results in growth and cell membrane changes. Related to Figure 2. (A) LC-MS/MS spectra showing CerPE lipids identified in *B. thetaiotaomicron* compared to the C12 Sphingosyl-PE standard. Spectra display the peaks of each CerPE eluted on a C8 column and the masses identified at a collision energy (CE) of 20MeV. The "A" and "B" labels on the spectra refer to the masses identified as the PE head-groups and Cer backbones, respectively. Corresponding predicted chemical structures are shown on the right. Representative transmission electron microscopy (TEM) images acquired on slides with negative staining of **(B)** BTWT and **(C)** BTΔSPT strains. The membrane of BTΔSPT could not be resolved to the level of BTWT and had a consistent black outline surrounding the bacteria. Magnifications range from 4,000 to 20,000x. Scale bars, 500 nm. Representative images taken from **(D)** BTWT or **(E)** BTΔSPT strains grown on a brain-heart infusion (BHI) agar plates supplemented with vitamin K and hemin. The average diameter of the colonies in the field of view is indicated below. **(F)** Growth curves over time of BTWT and BTΔSPT strains and the BTΔSPT strain complemented with the spt gene in BHI media, with OD600 plotted on the y-axis and time (h) on the x-axis.

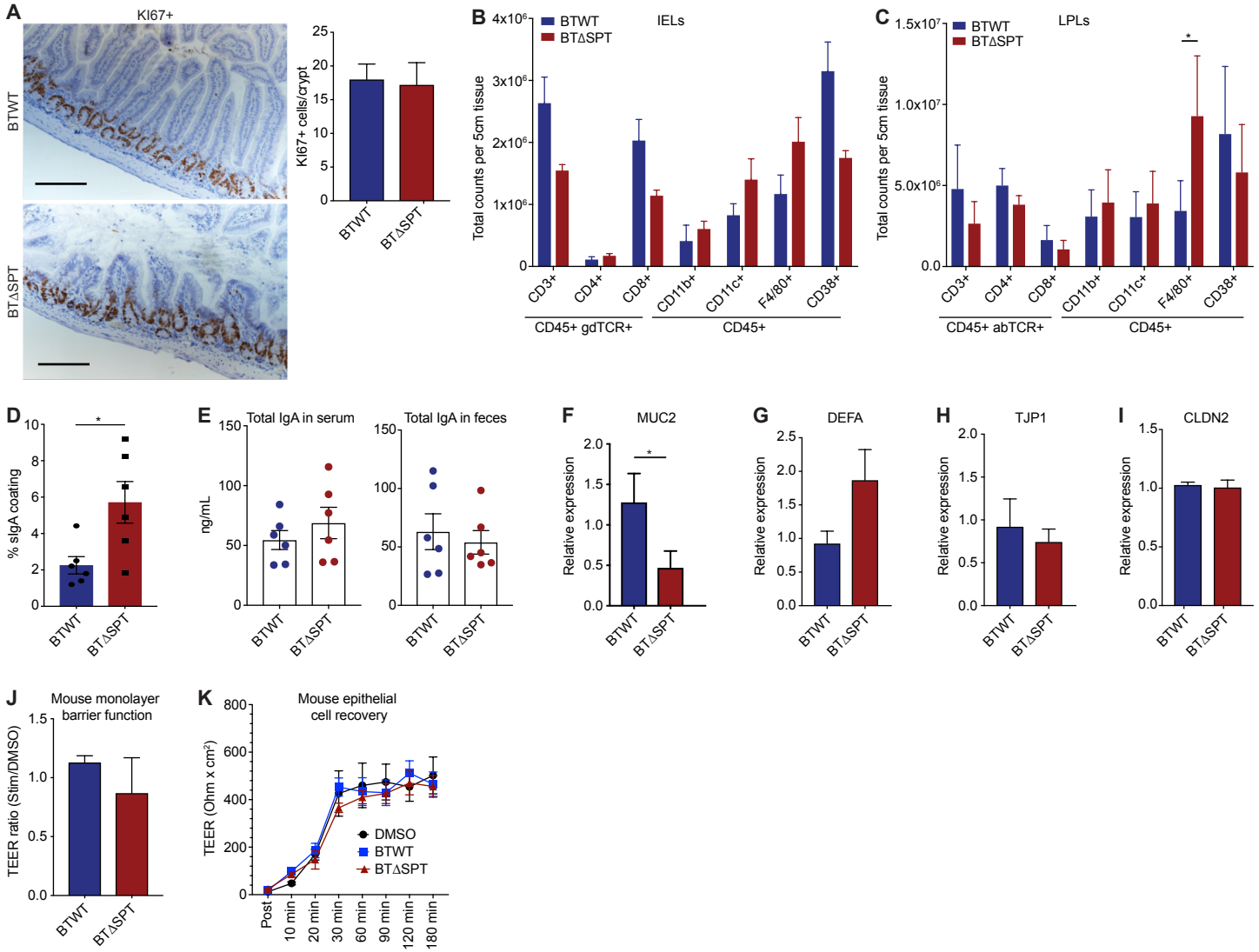

Figure S3: Presence of *B. thetaiotaomicron* sphingolipids influences innate immune responses and barrier function in mice. Related to Figure 3. (A) Representative images of ileal sections from germ-free mice colonized with the BTWT or BTΔSPT strain. Cells stained with KI67+ (brown) were mostly restricted to the crypts. Scale bars, 100 μm. The number of KI67+ cells per crypt in each sample were counted, normalized, and plotted showing no change. 25 crypts were counted per slide, n=6. Lymphocytes were isolated from the **(B)** intraepithelial region (IELs) or **(C)** lamina propria (LPLs) of the small intestine of BTWT-colonized (blue) and BTΔSPT-colonized (red) mice. The relative abundance of each cell type was plotted (y-axis) as a function of total amount per 5cm of intestinal tissue. T-cells were stained using antibodies for CD3, CD4, CD8, αβTCR and γδTCR, and granulocyte populations were stained using CD11b, CD11c, F4/80 and CD38 as an activation marker. **(D)** Fecal pellets from BTWT- and BTΔSPT-colonized mice were stained with a fluorescent antibody for IgA and analyzed on a flow cytometer to detect endogenous sIgA binding to each bacterium. The total percentage of sIgA-positive bacteria was quantified and plotted. **(E)** Concentration of IgA (ng/mL) as determined by ELISA in the serum or feces of each mouse. Data is representative of 2 independent experiments, n=6. Relative RNA expression of **(F)** *MUC2*, **(G)** alpha-defensin (*DEFA*), **(H)** tight-junction protein-1 (*TJP1*) and **(I)** claudin-2 (*CLDN2*) was quantified by qPCR from colonic tissue of BTWT- (blue) and BTΔSPT-colonized (red) mice. Relative expression (y-axis) was normalized between samples by GAPDH expression. **(J)** Permeability of monolayers stimulated with crude lipid extracts from BTWT (blue) or BTΔSPT (red). Monolayer permeability and barrier function for each sample (n=3) was expressed as TEER of the stimulated monolayer divided by TEER of the DMSO control (y-axis). **(K)** Calcium-chelated monolayers (TEER approaching zero) were stimulated with the same extracts as in (A) and changes in TEER were analyzed over 10- and 30-minute intervals. Each graph is representative of 2 independent experiments, n=3. Statistical analysis was performed using the Mann-Whitney U-test. *p<0.05. All error bars are +/- SEM.

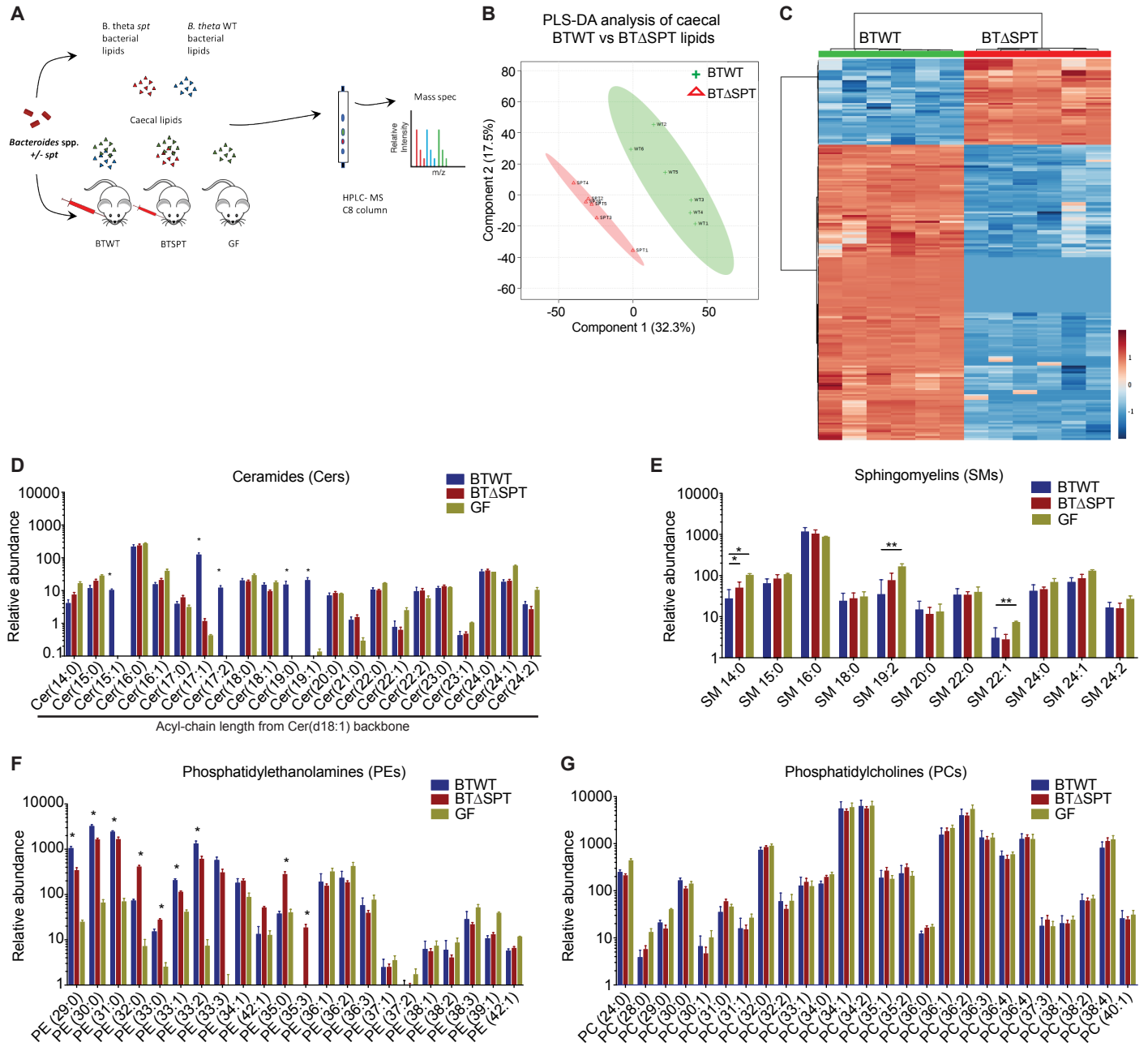

Figure S4: Lipidomic analysis of mouse caecal contents from mono-colonized and germ-free mice. Related to Figure 4. **(A)** Workflow utilized to determine whether a lipidomic feature was (i) bacterial- or host-produced, (ii) a sphingolipid and (iii) synthesized *in vivo*. **(B)** Partial-least squares discriminant analysis (PLS-DA) was performed on the lipidome from BTWT- (green) and BTΔSPT-colonized (red) mouse caecum, and the component change between each sample was plotted. Mouse caecal samples from each group clustered together. **(C)** The top 250 hits on the PLS-DA analysis were arranged in a heat-map, with upregulated lipids in red and downregulated lipids in blue, and samples clustered by Euclidean distance. Lipids from each group of mouse caecal samples again clustered together. Data is representative of 2 independent experiments, n=6. Relative abundances of the annotated sphingolipids detected in the caecum of BTWT- (blue), BTΔSPT-colonized (red) and germ-free (GF; green) mice were plotted and arranged in order of acyl chain length from smallest to largest (left to right) for **(D)** ceramides (Cers) and **(E)** sphingomyelins (SMs). Relative abundances of the annotated phospholipids detected in the caecum of BTWT- (blue), BT ΔSPT-colonized (red) and GF (green) mice were plotted and arranged in order of acyl chain length from smallest to largest (left to right) for **(F)** phosphatidylethanolamines (PEs), and **(G)** phosphatidylcholines (PCs). Data is representative of 2 independent experiments, n=6 per group for BTWT- and BTΔSPT-colonized mice and n=2 for GF mice. Statistical analysis was determined by analysis of the FDR (*FDR<0.05; **FDR<0.01; ***FDR<0.001). All errors bars are +/- SEM.

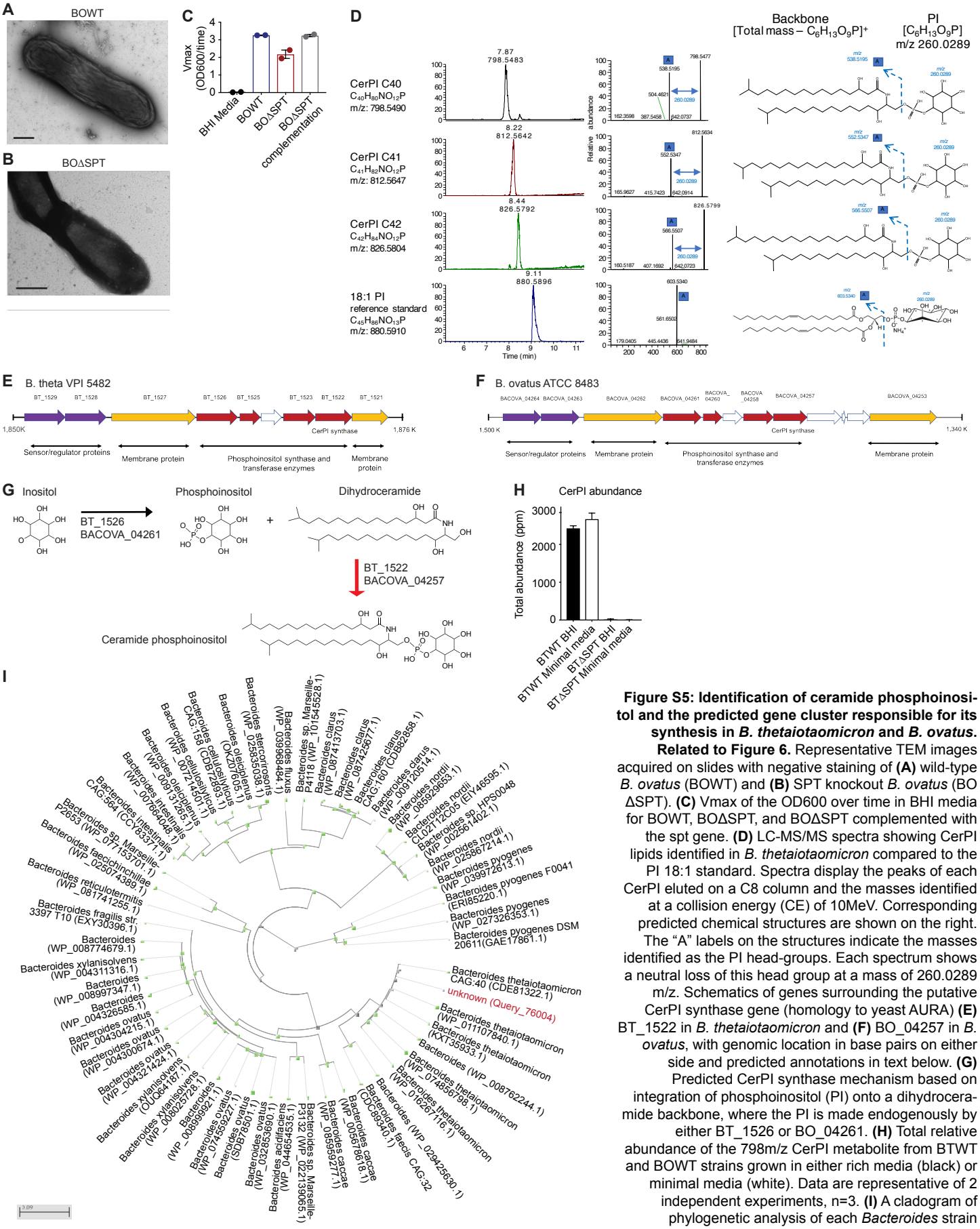

Figure S5: Identification of ceramide phosphoinositol and the predicted gene cluster responsible for its synthesis in *B. thetaiotaomicron* and *B. ovatus*. Related to Figure 6. Representative TEM images acquired on slides with negative staining of **(A)** wild-type *B. ovatus* (BOWT) and **(B)** SPT knockout *B. ovatus* (BO ΔSPT). **(C)** Vmax of the OD600 over time in BHI media for BOWT, BOΔSPT, and BOΔSPT complemented with the spt gene. **(D)** LC-MS/MS spectra showing CerPI lipids identified in *B. thetaiotaomicron* compared to the PI 18:1 standard. Spectra display the peaks of each CerPI eluted on a C8 column and the masses identified at a collision energy (CE) of 10MeV. Corresponding predicted chemical structures are shown on the right. The "A" labels on the structures indicate the masses identified as the PI head-groups. Each spectrum shows a neutral loss of this head group at a mass of 260.0289 m/z. Schematics of genes surrounding the putative CerPI synthase gene (homology to yeast AURA) **(E)** BT_1522 in *B. thetaiotaomicron* and **(F)** BO_04257 in *B. ovatus*, with genomic location in base pairs on either side and predicted annotations in text below. **(G)** Predicted CerPI synthase mechanism based on integration of phosphoinositol (PI) onto a dihydroceramide backbone, where the PI is made endogenously by either BT_1526 or BO_04261. **(H)** Total relative abundance of the 798m/z CerPI metabolite from BTWT and BOWT strains grown in either rich media (black) or minimal media (white). Data are representative of 2 independent experiments, n=3. **(I)** A cladogram of phylogenetic analysis of each *Bacteroides* strain containing the putative CerPI synthase gene (significant homology to yeast AURA). Scale of phylogenetic distance is indicated below. Strains were sequenced from human stool. All errors bars are +/- SEM.

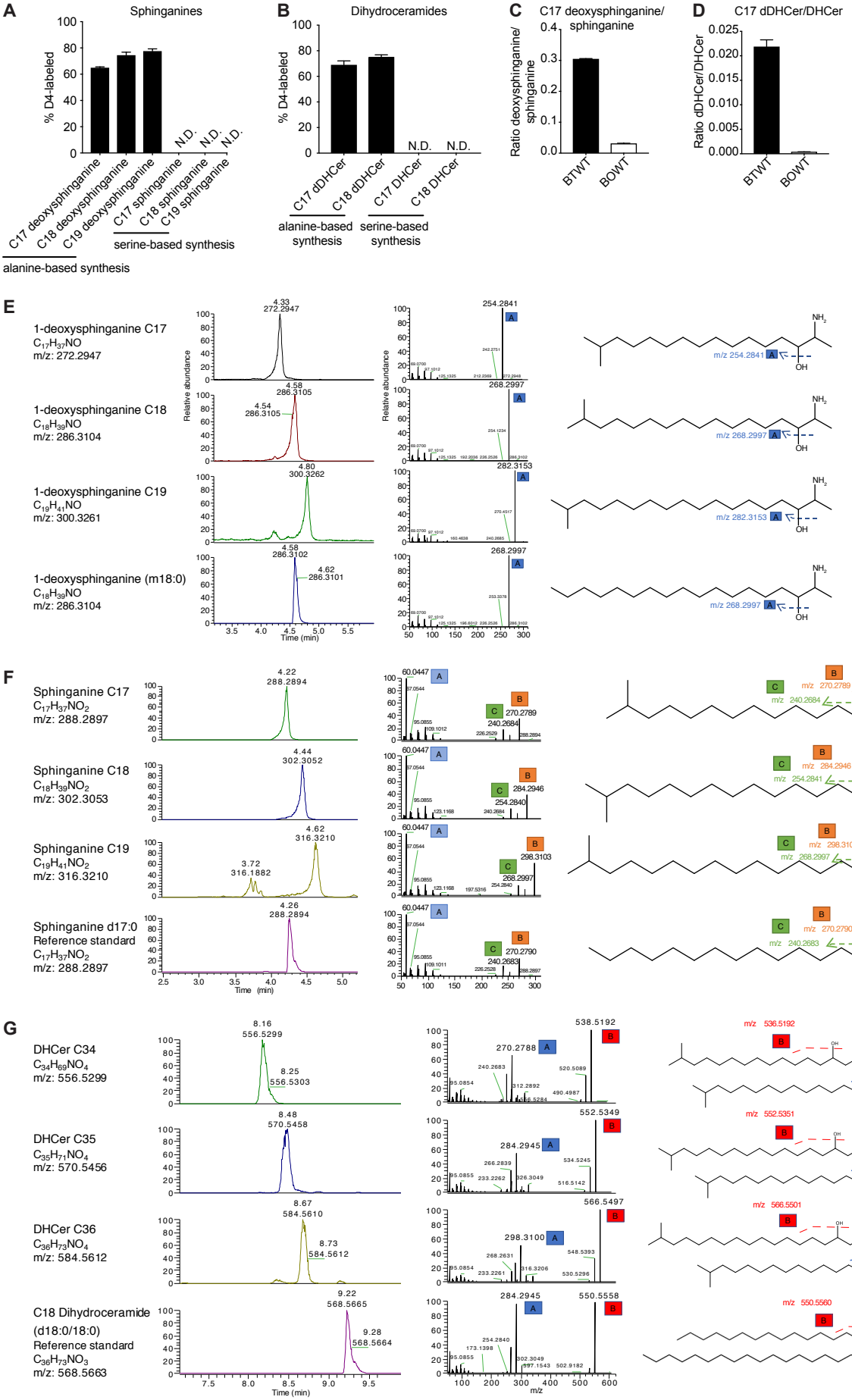

Figure S6: Isotopic alanine labeling and LC-MS/MS analysis reveal Spt is responsible for the enzymatic production of mammalian-like deoxysphingolipids and sphinganines in *Bacteroides*. Related to Figure 6. See legend on next page.

(*Figure S6 legend continued from previous page*.) BTWT was grown in a minimal media with D4-labelled alanine, and lipids were extracted and analyzed by LC-MS/MS. **(A)** Percentage of D4-alanine labeling compared to the total peak intensity of the mass measured for the three deoxysphinganine metabolites (alanine-based synthesis) and corresponding sphinganine metabolites (serine-based synthesis). **(B)** Percentage of D4-alanine labeling compared to the total peak intensity of the mass measured for the two deoxy-dihydroceramide metabolites (alanine-based synthesis) and corresponding dihydroceramide metabolites (serine-based synthesis). In each case, we observed a significant increase in deuterated labelling of the deoxysphinganines and deoxysphingolipids compared to their serine-based analogs and unlabeled controls. Data are representative of 3 biological replicates per group. The ratio between the abundance of **(C)** C17 deoxysphinganine over sphinganine and **(D)** C17 deoxydihydroceramide (dDHCer) over dihydroceramide (DHCer) was quantified for the BTWT (black) and BOWT (white) strains to assess the frequency of alanine- compared to serine-based sphingolipid synthesis. The higher ratio for the BTWT strain indicates a greater proportion of deoxysphingolipids are synthesized in these bacteria compared to BOWT. All errors bars are +/- SEM. **(E)** LC-MS/MS spectra showing masses identified in *B. thetaiotaomicron* annotated as 1-deoxysphinganine compared to a C18 deoxysphinganine purchased standard. Spectra display the peaks of different acyl chain lengths of deoxysphinganine eluted on a C8 column and the masses identified at collision energies (CE) of 30 MeV. Structures of the 1-deoxysphinganine standard and predicted structures from *B. thetaiotaomicron* corresponding to the masses identified in the MS/MS are shown on the right and are nearly identical. **(F)** LC-MS/MS spectra showing masses identified in *B. thetaiotaomicron* annotated as sphinganine compared to a C17 sphinganine commercial standard. Spectra display the peaks of different acyl chain lengths of sphinganine eluted on a C8 column and the masses identified at collision energies (CE) of 30 MeV. Structures of the sphinganine standard and predicted structures from *B. thetaiotaomicron* corresponding to the masses identified in the MS/MS are shown on the right and are nearly identical. **(G)** LC-MS/MS spectra showing masses identified in *B. thetaiotaomicron* annotated as dihydroceramide (DHCer) compared to a d18:0/18:0 DHCer commercial standard. Spectra display the peaks of different acyl chain lengths of DHCer eluted on a C8 column and the masses identified at collision energies (CE) of 20 MeV. Structures of the DHCer standard and predicted structures from *B. thetaiotaomicron* corresponding to the masses identified in the MS/MS are shown on the right.

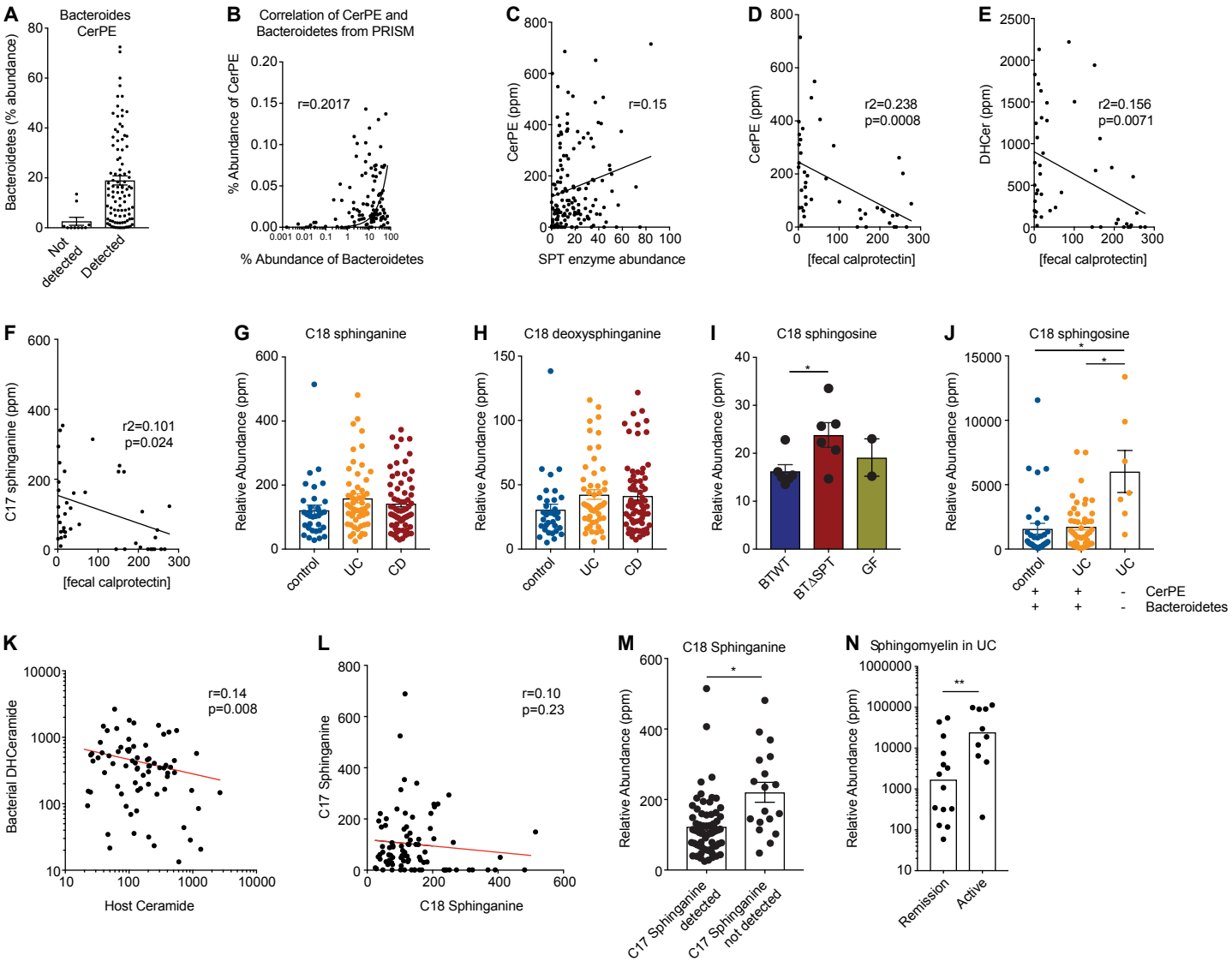

Figure S7: Significant correlations and differential abundances of bacterial and mammalian sphingolipids during IBD and increased intestinal inflammation in human subjects. Related to Figure 7. (A) Stool samples from non-IBD control, Crohn's disease (CD), and ulcerative colitis (UC) subjects in which no *Bacteroides* CerPE was detected were binned separately from the rest of the samples, and all samples were assessed for the presence of Bacteroidetes by metagenomics (% abundance). **(B)** The percentage abundance of CerPE per metabolite detected (y-axis) was plotted against the percentage abundance of Bacteroidetes in the corresponding sample (x-axis). This analysis revealed a positive correlation, using a line of best fit as displayed in black. **(C)** The relative abundance of the SPT enzyme by metagenomics analysis (x-axis) was plotted against the relative abundance of CerPE (y-axis), revealing a positive correlation as depicted by the linear line of best fit (Pearson's correlation coefficient). For each stool sample for which the data existed, the abundance (ppm) of **(D)** CerPE, **(E)** DHCer and **(F)** C17 sphinganine was plotted compared to the concentration of fecal calprotectin. Trend lines indicate directionality. Each analysis revealed a negative correlation by Pearson correlation coefficient and was statistically significant (r2 and p values indicated). C18 sphinganine and C18 deoxysphinganine are synthesized by both bacteria and mammalian cells. Relative abundances (ppm) of **(G)** C18 sphinganine and **(H)** C18 deoxysphinganine in the stool of non-IBD controls (blue), CD patients (red) and UC patients (yellow) were plotted and the mean of each group was compared. **(I)** A plot of C18 sphingosine abundance (ppm) in BTWT-colonized (blue), BTΔSPT-colonized (red) and germ-free (GF; green) mice. **(J)** To determine the impact of Bacteroidetes colonization on sphingosine abundance in stool, the relative abundance of C18 sphingosine was compared between control samples, UC samples, and UC samples without detectable CerPE and Bacteroidetes. **(K)** The correlation between bacterial-produced dihydroceramide abundance (y-axis) and mammalian-produced ceramide abundance (x-axis) was determined by plotting the relative abundance of each in a pool of control and UC stool samples. **(L)** The correlation between bacterial-produced C17 sphinganine abundance (y-axis) and mammalian-produced C18 sphinganine abundance (x-axis) was determined by plotting the relative abundance of each in a pool of control and UC stool samples. For each plot, a line was drawn to represent the linear correlation. Statistical analysis was performed using Pearson correlation analysis. **(M)** The relative abundance of C18 sphinganine (y-axis) was analyzed in samples where C17 sphinganine was and was not detected. **(N)** The relative abundance of all detected sphingomyelin lipids in the stool of UC patients during active disease (SCCI index > 5) and remission was plotted for the samples with this information. All correlation analysis was performed and quantified by using Pearson's correlation coefficient. Statistical analysis was determined by analysis of the FDR (*FDR<0.05; **FDR<0.01; ***FDR<0.001).

Table S1. Related to Figure 2. List of most differentially expressed genes of BTWT compared to BTΔSPT after growth in both minimal media (MM) and rich media (RM).

GENE	LOG_2 FC RM	LOG_2 FC MM	FDR	GENE NAME (KEGG NUMBER)
BT_0870	2.80	2.25	7.8E-82	Serine palmitoyltransferase (K00652)
BT_1574	2.03	2.96	1.1E-34	long-chain fatty acid transport protein (K06076)
BT_1655	4.54	-2.26	1.3E-139	hypothetical protein
BT_1724	3.20	-4.70	2.8E-94	hypothetical protein
BT_1725	2.85	-4.57	6.58E-32	transcriptional regulator
BT_1652	4.05	-1.15	9.3E-109	lipopolysaccharide biosynthesis protein
BT_1653	4.46	-1.55	8.4E-132	lipopolysaccharide biosynthesis protein
BT_1654	4.05	-1.85	1.9E-143	polysialic acid transport protein kpsD
BT_1656	4.42	-1.45	4.0E-141	transcriptional regulator
BT_2452	2.17	1.16	1.3E-13	hypothetical protein
BT_4039	-2.06	1.74	6.68E-29	SusC homolog
BT_4465	-2.65	-1.41	1.3E-18	Ca-activated chloride channel homolog (K07114)
BT_1040	2.32	1.11	4.6E-67	SusC homolog
BT_1648	4.09	-1.08	1.1E-106	glycosyltransferase
BT_2173	-3.17	-1.08	1.2E-39	hypothetical protein

Table S2. Related to Figure 5. List of 35 bacterial sphingolipids produced by *B. thetaiotaomicron* and *B. ovatus.*

RT_M/Z	CLASS	NAME	FORMULA	RELATIVE ABUNDANCE	DETECTABLE IN HUMAN STOOL?
4.12_286.2742	sphingolipid	3-ketosphinganine C17	$C_{17}H_{35}NO_2$	+	
4.36_300.2899	sphingolipid	3-ketosphinganine C18	$C_{18}H_{37}NO_2$	+	
4.55_314.3053	sphingolipid	3-ketosphinganine C19	$C_{19}H_{39}NO_2$	+	
3.88_272.2583	sphingolipid	3-ketosphinganine C16	$C_{16}H_{33}NO_2$	+	
4.08_288.2895	sphingolipid	Sphinganine C17	$C_{17}H_{37}NO_2$	++	Yes
4.34_302.3052	sphingolipid	Sphinganine C18	$C_{18}H_{39}NO_2$	++	Yes
4.50_316.3208	sphingolipid	Sphinganine C19	$C_{19}H_{41}NO_2$	++	Yes
3.87_260.2584	sphingolipid	Sphinganine C15	$C_{15}H_{33}NO_2$	+	
3.99_274.2739	sphingolipid	Sphinganine C16	$C_{16}H_{35}NO_2$	++	
4.84_330.3365	sphingolipid	Sphinganine C20	$C_{20}H_{43}NO_2$	+	
7.42_528.4987	sphingolipid	Dihydroceramide C32	$C_{32}H_{65}NO_4$	+	
7.69_542.5144	sphingolipid	Dihydroceramide C33	$C_{33}H_{67}NO_4$	++	
7.90_556.5301	sphingolipid	Dihydroceramide C34	$C_{34}H_{69}NO_4$	+++++	Yes
8.22_570.5457	sphingolipid	Dihydroceramide C35	$C_{35}H_{71}NO_4$	+++++	Yes
8.40_584.5613	sphingolipid	Dihydroceramide C36	$C_{36}H_{73}NO_4$	++++	Yes
8.50_598.5770	sphingolipid	Dihydroceramide C37	$C_{37}H_{75}NO_4$	++	
8.00_550.5197	sphingolipid	Ceramide C35	$C_{35}H_{67}NO_3$	+	
8.52_578.5507	sphingolipid	Ceramide C37	$C_{37}H_{71}NO_3$	+	
7.52_522.4881	sphingolipid	Ceramide C33	$C_{33}H_{63}NO_3$	+	
8.53_552.5352	sphingolipid	Ceramide C35	$C_{35}H_{69}NO_3$	+	
8.44_538.5194	sphingolipid	Ceramide C34	$C_{34}H_{67}NO_3$	+	
7.77_679.5382	sphingolipid	Ceramide phosphoethanolamine C36	$C_{36}H_{75}N_2O_7P$	++++	Yes
7.56_665.5226	sphingolipid	Ceramide phosphoethanolamine C35	$C_{35}H_{73}N_2O_7P$	+++	Yes
8.04_693.5538	sphingolipid	Ceramide phosphoethanolamine C37	$C_{37}H_{77}N_2O_7P$	++++	Yes
7.29_651.5072	sphingolipid	Ceramide phosphoethanolamine C34	$C_{34}H_{71}N_2O_7P$	++	
8.30_707.5695	sphingolipid	Ceramide phosphoethanolamine C38	$C_{38}H_{79}N_2O_7P$	+	
7.41_798.5486	sphingolipid	Ceramide phosphoinositol C40	$C_{40}H_{80}NO_{12}P$	++++	Yes
7.72_812.5626	sphingolipid	Ceramide phosphoinositol C41	$C_{41}H_{82}NO_{12}P$	++++	
7.98_826.5788	sphingolipid	Ceramide phosphoinositol C42	$C_{42}H_{84}NO_{12}P$	+++	
4.21_284.2945	deoxysphingolipid	1-deoxy-ketosphinganine C18	$C_{18}H_{37}NO$	+	
4.22_272.2946	deoxysphingolipid	1-deoxysphinganine C17	$C_{17}H_{37}NO$	+	Yes
4.48_286.3103	deoxysphingolipid	1-deoxysphinganine C18	$C_{18}H_{39}NO$	+	Yes
4.69_300.3259	deoxysphingolipid	1-deoxysphinganine C19	$C_{19}H_{41}NO$	+	
8.53_540.5358	deoxysphingolipid	deoxy-dihydroceramide C34	$C_{34}H_{69}NO_3$	++	Yes
8.72_554.5511	deoxysphingolipid	deoxy-dihydroceramide C35	$C_{35}H_{71}NO_3$	++	Yes